Temporal Variations in the Scaling Properties of Rain Echoes during the Development of a Cold Low in Saskatchewan

R. G. LAWFORD*

Climate Processes and Earth Observation Division, Atmospheric Environment Service, National Hydrology Research Centre, Saskatoon, Saskatchewan, Canada

(Manuscript received 16 May 1995, in final form 10 December 1995)

ABSTRACT

A better understanding of the scaling properties of rain could assist in parameterizing rain events in hydrological models and support the development of improved "weather generators." A technique developed for the analysis of the scaling characteristics of snow patches during melt has been adapted to study the development of rain echoes observed by radar. The technique is applied to echo ensembles detected by a weather radar located at Elbow, Saskatchewan, for a 48-h period from 1800 LST 30 June to 1800 LST 2 July 1991.

The scaling properties and other statistical measures of ensembles of radar echoes from 2-km MSL CAPPI (constant-altitude plan position indicator) maps were analyzed for a 240 km × 240 km square domain centered on Elbow. The 0.2 mm h^{-1} rain rate was used to define the echoes. During the 48-h period, the sizes, numbers, and shapes of echoes within the domain changed considerably as a result of a cold low that intensified just outside the study area and then moved eastward. Analyses of some scaling properties of these ensembles were carried out along with tests of their sensitivity to reflectivity threshold.

The echo ensembles were characterized by the perimeter/area and Korcak parameters. The perimeter/area parameter provides a measure of the "roughness" of the edges of the echoes. Values of the perimeter/area parameter from this study agreed well with the results obtained by other investigators who used different data sources and techniques. The Korcak parameter, which represents the "clumpiness" of the pattern, was more variable. Changes in this parameter may serve as a precursor to significant changes in the overall rain pattern. Both the statistical properties and the scaling properties of echo ensembles were found to vary depending on the effects of the dynamic and thermodynamic atmospheric controls on rain formation.

1. Introduction

Over the past decade there has been growing interest in relating rain amounts averaged over large areas to rain amounts measured over much smaller areas or at points. In order to effectively use outputs from GCMs and NWP models, hydrologists require techniques to relate the 24-h values of rain from model grid squares to rain amounts over smaller areas and for shorter periods of time. Generally, hydrological models produce better results when they incorporate the time variability of rain. This implies that there is considerable value in improving techniques to characterize and model the space–time variability of rain events.

Rainfall is commonly represented in hydrological models by statistical distributions. However, many radar studies (Chisholm and Renick 1972; Browning et al. 1973) suggest that precipitation patterns possess some degree of organization because the shapes of rain areas are dependent on the atmospheric processes influencing their development. For example, the shape of a rain pattern depends on whether the rain formed at the top of a convection column and then fell to the ground, producing a relatively small bounded area with maximum rain intensities in the pattern, or developed in stratiform clouds resulting in a relatively uniform distribution of rain over an extensive area with occasional local maxima, or formed under dissipating cumulonimbus cloud tops where ice crystals falling from higher levels seeded the underlying clouds.

A number of studies (e.g., Lovejoy and Schertzer 1991; Over and Gupta 1994) have demonstrated that the space and time variability in cloud and rain patterns can be described as multiscaling or multifractal. These results suggest that some order exists in the development and interactions of elements within a rain pattern over time. The multiscaling properties of rain have been used by Gupta and Waymire (1993) and Over and Gupta (1994) in modeling rain with random cascade generators. Other approaches to modeling spatial rainfall patterns have relied on morphologically based algorithms for upscaling and downscaling rain patterns (Kumar and Foufoula-Georgiou 1994).

* Current affiliation: GCIP Office, NOAA/Office of Global Programs, Silver Spring, Maryland.

Corresponding author address: R. G. Lawford, GCIP Office, Suite 1225, NOAA/OGP, 1100 Wayne Avenue, Silver Spring, MD 20910.

Although the resolution of weather radar is limited by the physical characteristics of its beam and its limited ability to sample at scales necessary to establish a relationship between mesoscale predictability and synoptic-scale atmospheric conditions (Zawadzki et al. 1994), radar data do provide an opportunity to study spatially continuous rain patterns over scales of importance to hydrologists. This study is intended to determine if variations in simple scaling parameters derived from radar rainfall patterns can be explained in terms of changes in large-scale atmospheric conditions.

The area covered by cloud and rain is an important parameter in modeling spatial distributions of rain and interpreting satellite imagery. Procedures have been developed to allow climate models to incorporate the fractional area covered by rain in computing the spatial variability of rainfall at the subgrid scale (Entekhabi and Eagleson 1989). Johnson and Smith (1990) reported that the relationship between rainfall volume and storm cloud area is close to linear, suggesting that it may be possible to estimate rain volumes from the area of cloud seen by satellite. Identification and analysis of geometric properties of rain patterns that are conserved with time could be useful for improving parameterizations of cumulus clouds in numerical weather prediction models and for validating relationships between cloud area and rain volume in a semiarid, high-latitude summer climate.

The present study documents the time variations in the scaling properties of low-level rain patterns and assesses how these variations are related to changing synoptic conditions. It focuses on the statistical and scaling properties of entire rain echo ensembles as they change over time. In order to consider the variations in scaling properties over a wide range of conditions, this study examines rain fields during a transition from a synoptic situation dominated by a cold low to one characterized by mesoscale and local convection. The analyses presented here may also serve as a basis for testing the ability of spatiotemporal rainfall models to simulate rain patterns for a range of meteorological conditions.

2. Analytical procedure

In this study, relevant statistical parameters for an ensemble of radar rain echoes including the area covered by echo, total rain flux, and the number of echoes were analyzed for a 48-h sequence of CAPPI (constant-altitude plan position indicator) maps. In addition, scaling properties were analyzed for each echo ensemble. The analytical techniques used in this study have been adapted from software developed by Shook (1993) based on properties of geometric shapes described by Mandelbrot (1983). Shook successfully applied these techniques to characterize geometric patterns of snow and no-snow areas during melt.

Scaling properties were calculated for echo ensembles on 2-km CAPPI maps. (A CAPPI map is a derived radar map that shows the distribution of rain at a fixed altitude and for a particular time). An echo is defined as a connected area of rain that appears on an individual CAPPI map. Echoes were defined for a number of rain intensity thresholds, although most of the analyses presented here are based on the 0.2 mm h^{-1} threshold. The number of echoes in ensembles with the 0.2 mm h^{-1} threshold ranged from 17 to 97 echoes. The average number of echoes per ensemble was 48.

The two scaling parameters discussed in detail in this paper are the perimeter/area parameter D_p and the Korcak parameter D_k. The computation of these parameters is based on the geometry of the rain pattern where a specific rain intensity threshold is used as the criteria for distinguishing between echo and no-echo pixels (i.e., pixels with an intensity level less than the threshold values were considered as no-echo pixels). The technique used for computing scaling exponents in this study requires at least two echoes to be present on each CAPPI map before values can be computed. Since at least 17 echoes were present in all ensembles with the 0.2 mm h^{-1} threshold, the number of echoes was not a problem unless it is explicitly noted in the text.

Schertzer and Lovejoy (1987) and Lovejoy and Schertzer (1990) have shown that important information can be derived from a multifractal analysis of precipitation datasets. An analysis of the multifractal properties of these radar echoes that includes a consideration of the influence of rain intensity has been carried out by Wang and Lawford (1994) using techniques described by Reyni (1970) and Halsey et al. (1986). Their results indicate that the scaling of precipitation on these days was weakly multifractal, which gives confidence in the utility of the rather simple approach reported here.

The perimeter/area parameter is calculated from the relationship:

$$P = C_1 A^{D_p/2},$$

where P is the perimeter of an echo, A is the area of an echo, C_1 is a constant related to the area of the smallest echo, and D_p is a scaling exponent (value of D_p is greater than or equal to 1.0).

The scaling exponent D_p characterizes the "roughness" of the edge of an object. Theoretically, the value for smooth edges such as the edges of rectangles and circles is 1.0. As shown by experimentation with different geometric shapes, the value of D_p increases to values as large as 1.8 when the edge becomes very "undulating and ragged" (see Fig. 1).

In order to compute the values of D_p using Shook's technique, a "bug" proceeded around the outside of each echo and recursively searched each pixel to determine if it was on the perimeter of an echo. As it progressed, it kept an accumulated total for the perimeter of that echo plus all the echoes it had previously circumscribed. It also looked inside the echo to find "donut holes," and when these existed, it added the

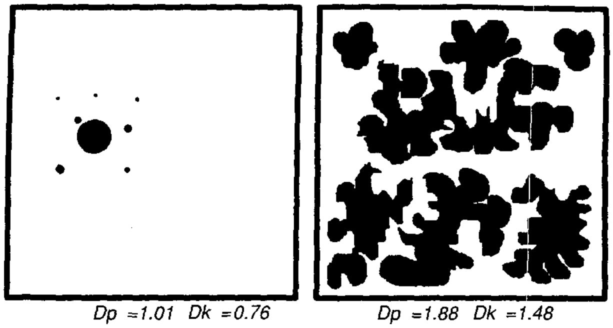

FIG. 1. Different synthetic echo patterns and the associated values of D_p and D_k. The scaling exponent D_p characterizes the "roughness" of the edges of the objects (increasing values occur for undulating and ragged edges); D_k is a scaling exponent that represents the relative frequency of objects having an area greater than a prescribed threshold (increasing values indicate a greater relative number of objects having similar areas).

perimeters of these interior holes to the echo's perimeter.

Korcak formulated an expression for the size distribution of objects that was modified to the form of a power-law relationship by Mandelbrot (1983). The scaling exponent in this relationship, D_k, hereafter referred to as the Korcak parameter, is dependent on the relative frequency of objects or echoes having an area greater than a prescribed threshold. The relationship, sometimes called the "number area" law, can be written as

$$F(A) = C_2 A^{-D_k/2},$$

where $F(A)$ is the fraction of objects whose area is equal to or greater than A, C_2 is a constant, and D_k is the Korcak parameter (Shook 1993).

Korcak's parameter is a measure of the concentration of area in a few large entities (or echoes). Experimentation, by the author, with different geometric patterns showed that when the value of D_k is small (0.5–0.8), there is generally one very large entity and a few smaller entities. On the other hand, when the influence of the largest entity is less overwhelming because it is closer in size to the other entities and the number of smaller entities is larger, the values of D_k are larger (1.3–2.0). Hence, increasing values of D_k suggest that there is a more uniform distribution of echo areas. Figure 1 shows examples of the geometric patterns that result in large and small values of D_p and D_k.

3. Data description

The analyses reported here are based on 377 radar echo ensembles observed during a 48-h period from 1800 LST 30 June 1991 to 1800 LST 2 July 1991. The time period was chosen because it satisfied the following criteria:

- both extensive and moderate echo coverage occurred and there was a transition from widespread rain to small intense rain cells during the period;
- the data for the period are relatively complete;
- the radar data are supported by other synoptic data that help in the interpretation of the dynamic and thermodynamic aspects of storm systems.

The Elbow weather radar is a C-band (5 cm) Enterprise system that collects volume scans every 6.5 min. The area under surveillance is shown in Fig. 2. CAPPI maps at 2 km MSL (generally 1.4 km above ground) were used in this analysis. Ground echo was eliminated by animating the maps and removing small echoes in the vicinity of the radar that remained stationary for periods of 1 h or longer. The CAPPI maps were then "masked" with a 240 km × 240 km square domain centered on Elbow. Only those echoes or portions of echoes within the domain were included in the analysis. As a result, only rain echoes observed within distances of 170 km of the radar are considered in this analysis. While rain at larger ranges is also detected by the radar, attenuation of the returned signals from rain at distances greater than 170 km make those rain intensities somewhat unreliable.

In this study, rain intensity thresholds (R) are used to define the echoes. The radar measures reflectivity values that are converted to rain intensities using the relationship: $Z = 200R^{1.6}$ (Marshall and Palmer 1948). The Marshall–Palmer relationship is also the basis for

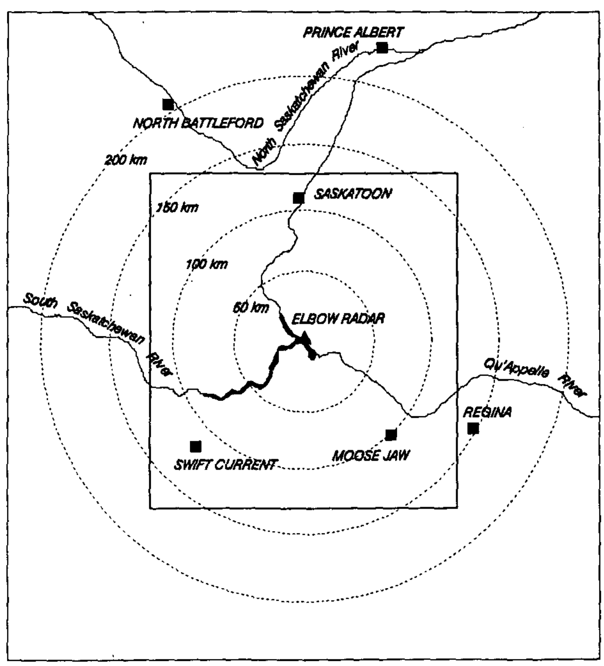

FIG. 2. Area under surveillance by the Elbow radar and the boundaries of the square domain used to extract data for this study.

rain flux calculations. CAPPI maps were analyzed for echoes with intensity threshold values of 0.2, 0.5, 1, 2, 5, and 10 mm h^{-1}. Figure 3 shows the CAPPI map for 1200 LST 1 July with precipitation intensity thresholds of 0.2 and 2 mm h^{-1}. It should be noted that the analyses presented in sections 6, 7a, and 7b of this paper are based on a rain intensity threshold of 0.2 mm h^{-1}.

For each CAPPI map, the following statistics were calculated: area of the domain covered by echo, rain flux, the total number of echoes, and the number and areal coverage of echoes exceeding certain sizes. As described in the previous section, D_p and D_k were also computed and their time variations throughout the 48-h period were analyzed. In addition to analyses for different intensity thresholds, the procedure was repeated using only echoes with areas greater than 200 km^2 (at an intensity threshold of 0.2 mm h^{-1}). In order to smooth some of the variability that existed between CAPPI maps, graphs were prepared for 1-h centered moving averages of each parameter.

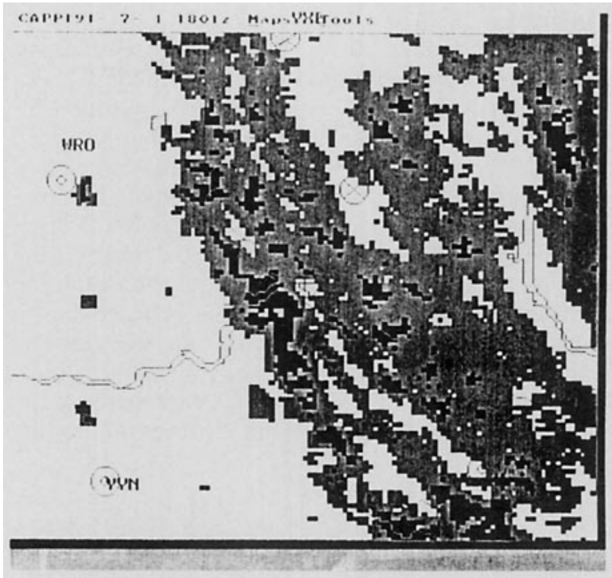

FIG. 3. Echo patterns on the CAPPI map for 1200 LST 1 July for the 0.2 and 2 mm h^{-1} intensity thresholds.

4. Factors influencing the interpretation of results

There are several possible sources of uncertainty in this analysis. The technique used to find the echo edge introduced some uncertainty into the values of the perimeter/area parameter. These uncertainties could amount to approximately one pixel in the perimeter length of each echo. Given the size of most perimeters, this uncertainty would not affect the overall results significantly except, possibly, for ensembles where a large number of small echoes was present. In addition, the pixel size of 2 km $\times$ 2 km limited the ability of the technique to resolve small-scale variability.

Another possible source of uncertainty in this study arose from echoes that overlapped the eastern and southern sides of the domain between 1200 LST 1 July and 0000 LST 2 July. As a result of the masking process, the edges of echoes overlapping the boundary of the study area were treated as straight edges, hence, the perimeter and, in turn, the perimeter/area parameter D_p were reduced when overlap occurred. However, as shown in section 7a, this effect was negligible.

The size of the domain may have influenced the values of the Korcak parameter. Shook (1993) showed that the Korcak parameter is sensitive to the size of the study area. He noted that a small study area may contain only a few large patches. However, in this study, the total number of echoes remained relatively large for an intensity threshold of 0.2 mm h^{-1}, with the exception of one 15-min period around 1600 LST 1 July when the number fell below 20, consequently, the values of D_k should be reliable. However, for analyses involving higher intensity thresholds ($\geqslant$5 mm h^{-1}) or large-area echoes only ($\geqslant$200 km^2), the number of echoes was smaller and more uncertainty was associated with the values of the scaling exponents.

Another minor uncertainty in this dataset arises from the radar system. It appears from inspection of radar maps from other days that there may be some beam blockage of 1°–2° width at 330° azimuth for the Elbow radar. This blockage could result in reduced reflectivities along this azimuth. Since relatively little rain occurred along this azimuth on the days being studied (the majority of rain was in the eastern sectors), the author believes that this factor did not affect the results in any significant way.

5. Synoptic situation

Since the attributes of the precipitation patterns are strongly influenced by the atmospheric conditions, the following synoptic overview provides relevant background for understanding the temporal changes in the rain patterns. During the 48-h period examined in this study, the weather pattern over the Canadian prairies was characterized by a trough and a cold low that developed on 1 July as it moved eastward through Saskatchewan and Manitoba. This system was followed by a northerly flow of drier air over the region in which mesoscale and localized convective storms developed.

At the beginning of the period (1800 LST 30 June), a trough with warm air aloft (TROWAL) extended northward from a low pressure system and an associated frontal wave centered on the eastern border of South Dakota. A ridge of high pressure was present over the Rocky Mountains.

During the next 24 h, the high pressure system moved southeastward along the mountains allowing a slow-moving trough line and cold low to dominate the synoptic regime over southeastern Saskatchewan and southern Manitoba. The convergence associated with this low and its trough in Saskatchewan led to the formation of a small secondary low just to the west of Regina at 1800 LST 30 June. This low persisted and slowly moved eastward into western Manitoba as it developed into a distinct low pressure center by 1200 LST (1800 UTC) 1 July (see Fig. 4a). Although a surface baroclinic zone was not apparent in the circulation around this low, there was a significant amount of low-level convergence associated with the system that led to the development of extensive cloud and rain over the study area during the morning of 1 July. Early in the afternoon of 1 July, the low pressure system moved eastward, causing surface winds over the study area to back to the north and to advect drier air into the area. The effects of this drier air combined with the warming of the surface, its associated boundary layer mixing and a weakening of the low-level convergence contributed to the rapid breakup of the rain pattern during the afternoon of 1 July.

The effects of the trough and its associated convergence were very evident in CAPPI map animations on 1 July. Echo development appeared to be associated with the zone of strong convergence and echo motions were clearly related to the direction of flow on either side of the line of maximum convergence. To the southwest of this line, echoes moved from northwest to southeast, while they moved north-northwestward to the northeast of the line. By 1800 LST 1 July, the line of maximum convergence had passed eastward out of the region and the main part of the large-scale rain system over Saskatchewan had dissipated.

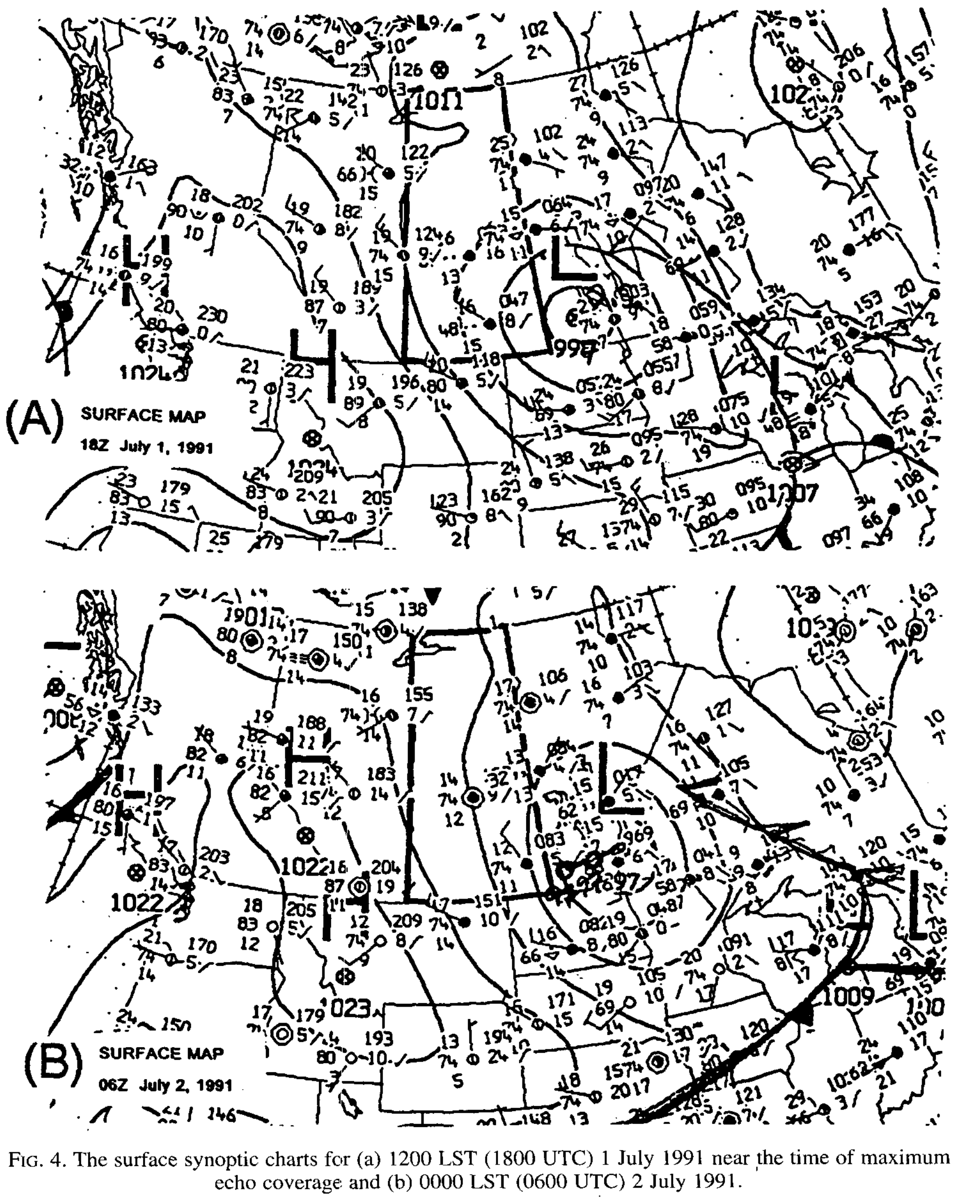

FIG. 4. The surface synoptic charts for (a) 1200 LST (1800 UTC) 1 July 1991 near the time of maximum echo coverage and (b) 0000 LST (0600 UTC) 2 July 1991.

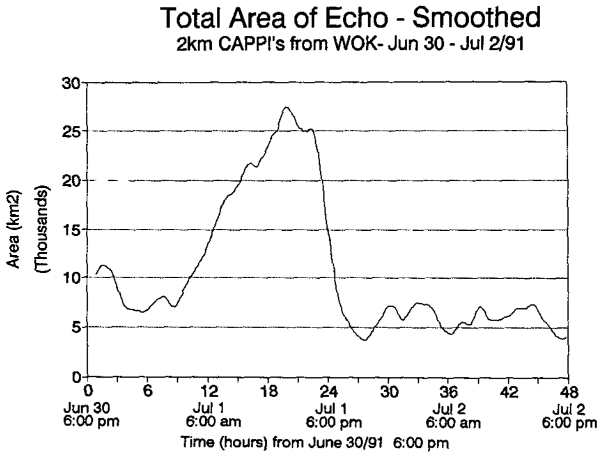

FIG. 5. Moving average variations in the areal coverage of echo for a rain intensity threshold of 0.2 mm h^{-1} during a 48-h period from 1800 LST 30 June to 1800 LST 2 July 1991. Moving averages were obtained from a 1-h centered running mean calculation.

The mean sea level (MSL) pressure chart for 0000 LST 2 July 1991 (0600 UTC 2 July) is shown in Fig. 4b. During 2 July, a high pressure system influenced Montana and southern Alberta and gradually spread into Saskatchewan. By 0000 LST 3 July, most of the echoes over the study area had dissipated.

The developing low pressure system at the surface on 1 July was associated with cyclonic flow at 500 mb. During 1 July, a center of low geopotential heights initially located on the Manitoba–Saskatchewan border deepened and moved into southern Manitoba. Cold-air advection occurred over Saskatchewan in the midtroposphere by 1800 LST 1 July, tending to decrease the stability of the lower atmosphere over the study area.

In summary, the first 12 h of the study period were characterized by strong low-level convergence over the area associated with a developing, slow-moving cyclonic system near the Saskatchewan–Manitoba border. However, as this system moved eastward, it brought dry-air advection and reduced the low-level convergence over the study area. The combination of these factors was conducive to the development of convective storms rather than widespread precipitation systems during the middle and latter parts of the period. However, as a high pressure system built eastward from Alberta throughout 2 July, it tended to stabilize the air mass and to suppress the convective activity late that afternoon.

6. Description of echo development

With the exception of the period between 0500 and 1700 LST 1 July and a brief period at the beginning of the study, the total area of echoes during the 48-h period included in this study ranged from 3.75×10^3 to 7.5×10^3 km^2. The rapid increase in area during a 12-h period commencing at 0500 LST 1 July was a result of the convergence and upward vertical motion associated with the development of the cold low described in the previous section.

Figure 5 shows the 1-h moving average for the total area of echo over the domain (240 km × 240 km) during the 48-h period. As noted earlier, smoothed time series were obtained by computing 1-h centered moving averages. During the period between 0200 and 1310 LST 1 July, the echo area increased at 2026 $km^2\ h^{-1}$ to a peak areal coverage of 29 040 km^2 (approximately 50% of the study area). Figure 4a, which shows the synoptic map for 1200 LST 1 July, indicates that a strong cyclonic flow was present over the eastern part of the study area 1 h before the time of maximum echo coverage. The peak areal coverage was followed by a very rapid decrease in total echo area of 4137 $km^2\ h^{-1}$ to a minimum of 3180 km^2 by 2125 LST. During the remainder of 1 July and the following day, the area covered by echo ranged from as little as 3180 to as much as 8020 km^2. This result suggests that the upper limit of instantaneous rain coverage over an area during periods dominated by convection is 14%, and it generally ranges from 7% to 12%.

In assessing the spatial patterns of rain, it is useful to know the proportion of area covered by large echoes. For the purposes of this analysis, a large echo is defined as one with an area greater than or equal to 4000 km^2. The proportion of echo coverage associated with large echoes varied dramatically throughout the 48-h period. During the early part of the period, more than 50% of the coverage came from large echoes. In particular, when the area of echo was increasing rapidly between 0500 and 1300 LST 1 July, 70%–95% of this coverage was associated with large echoes. The proportion of the area covered by large echoes decreased as the total rain area decreased between 1310 and 2105 LST 1 July. Inspection of the CAPPI maps indicated that the re-

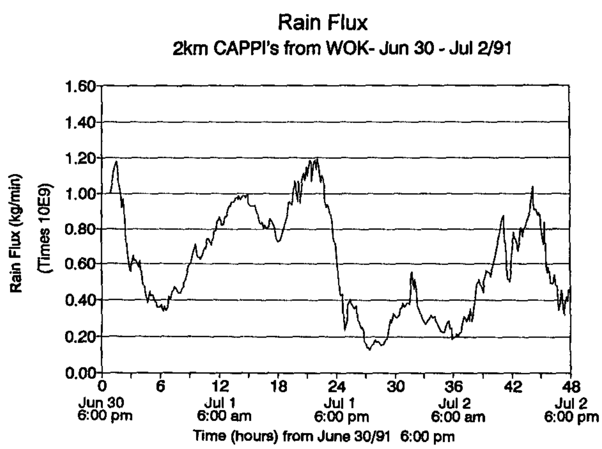

FIG. 6. Variations in the rain flux during a 48-h period from 1800 LST 30 June to 1800 LST 2 July 1991.

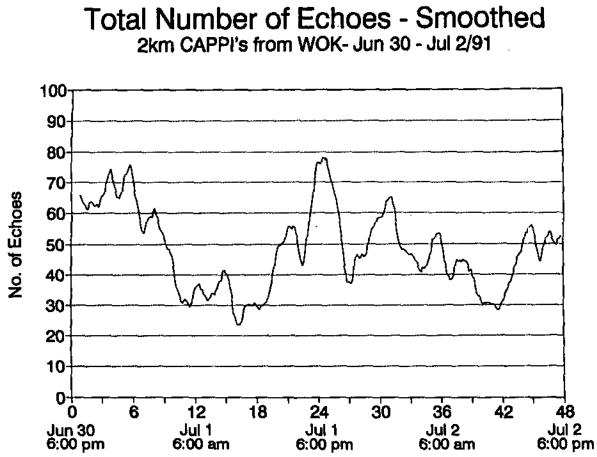

FIG. 7. Moving average variations in the number of echoes for a rain intensity threshold of 0.2 mm h^{-1} during a 48-h period from 1800 LST 30 June to 1800 LST 2 July 1991. Moving averages were obtained from a 1-h centered running mean calculation.

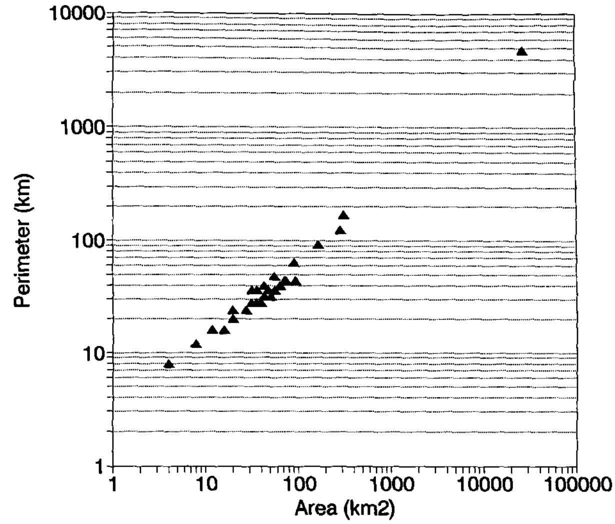

FIG. 8. Graph showing the plot of log area against log perimeter for 1310 LST 1 July 1991 (the time of maximum echo coverage).

duction in echo area was due primarily to the dissipation of the larger rain areas.

Time variations in the rain flux in units of billions of kilograms per minute were estimated by using the Marshall–Palmer equation (given in section 3). The results are shown in Fig. 6. Values of the rain flux were obtained by aggregating the rain rates over each pixel and converting them from millimeters per hour to kilograms per minute. In the unsmoothed data, the total rain flux ranged between 0.18×10^9 and 1.2×10^9 kg min^{-1} for the 48-h period. Peaks occurred near 1900 LST 30 June, 1600 LST 1 July, and 1400 LST 2 July. The rapid development of the echo area that began at 0300 LST 1 July was accompanied by a large increase in rain flux that reached a relative maximum of 1.0×10^9 kg min^{-1} at 0800 LST 1 July, then subsided until 1200 LST and subsequently built to a second relative maximum at 1600 LST (3 h after the maximum rain area occurred). The second maximum was associated with the formation of smaller cells with higher rain intensities. The peak average rainfall rate over the entire domain was approximately 1.25 mm h^{-1} or 3 cm day^{-1}.

The total number of echoes ranged from a low of 17 at 0940 LST 1 July to a maximum of 97 at 1756 LST on the same day. The smoothed time variations in the total number of echoes over the 48-h period are shown in Fig. 7. The peak in the number of echoes lagged the maximum area of echo by almost 6 h and occurred 2–3 h after the times of maximum surface temperature recorded at automatic weather stations within the study area (Strong 1994, personal communication). A rapid increase in the number of echoes occurred as the percentage area covered by large area echoes decreased after 1500 LST 1 July, which supports the hypothesis that the increase in the number of echoes was associated with the breakup of large echoes rather than the formation of new storms. While there were distinctive differences between the afternoons of 1 July and 2 July, the total number of echoes increased during both afternoons (howbeit the increase was more dramatic on 1 July).

An analysis of the number of echoes as a function of echo size indicated that the largest percentage of echoes in the 400–2000-km^2 range occurred during the afternoons. The percentage number of echoes with areas exceeding 4000 km^2 ranged from 0% to 12%. The time intervals when the percentages of very large echoes ($\geqslant$4000 km^2) were greater than 6%, persisted from

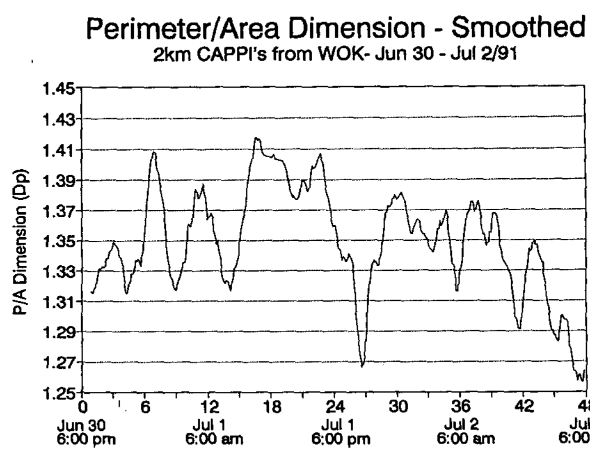

FIG. 9. Moving average variation in the perimeter/area parameter D_p over a 48-h period from 1800 LST 30 June 1991 to 1800 LST 2 July 1991. Moving averages were obtained from a 1-h centered running mean calculation.

TABLE 1. Comparison of the perimeter/area parameter values calculated in this study and the similar dimensions computed in other studies for other datasets.

Author	D_p	Description
Lovejoy (1982)	1.35 ± 0.05	Cloud and rain patterns over a wide range of scales
Rys and Waldvogel (1986)	1.36 ± 0.1 ($A > 8$ km^2)	Radar maps of hailstorms
	1.0 ± 0.1 ($A < 8$ km^2)	
Hentschel and Procaccia (1984)	$1.37 < D_p < 1.41$	Theoretical computations based on fractally homogeneous turbulence
This study	1.35 ± 0.04	Radar CAPPI maps for a 48-h interval

1000 to 1200 LST 1 July and from 0900 to 1200 LST 2 July.

7. Scaling properties

a. Perimeter/area parameter

As indicated in section 2, the perimeter/area parameter D_p, which is a measure of the "roughness" of the edges of echoes, was computed for each CAPPI map. The value of D_p was obtained by plotting the log of perimeter against the log of area for each echo in a given ensemble and then finding the slope of the line of best fit. The perimeters and areas of individual echoes for 1310 LST 1 July, the time of maximum echo coverage, are shown in Fig. 8. The slope of a line of best fit passing through these points is 0.69, giving a value for D_p of 1.38. The goodness of fit for this regression line is indicated by r^2, the proportional reduction in the sum of squares attributable to the regression of the log of the echo perimeter on the log of the echo area. The value of r^2 for this graph is 0.98, indicating that the regression line explains virtually all of the variance associated with these data points. The same procedure was carried out for each of 377 echo ensembles. The average value of D_p was 1.35, with a standard deviation of 0.04.

The values of D_p varied between 1.22 and 1.46 during that interval. The goodness of fit was indicated by r^2, which had an average value of 0.98 for the 48-h period of study. Furthermore it remained relatively constant throughout the entire period, indicating that the goodness of fit was very high for all values of echo numbers and areas.

Figure 9 shows the moving average values of D_p for echo ensembles with a 0.2 mm h^{-1} reflectivity threshold. During the afternoons of 1 and 2 July, the value of D_p decreased between 1500 and 2000 LST 1 July and between 1500 and 1800 LST 2 July. This decrease may have occurred because the boundary layer was a source of thermals that could have led to the formation of a number of smaller relatively circular echoes. According to Fig. 9, the largest value of D_p occurred at 1100 LST 1 July at a time when echo area was increasing quite rapidly. However, the fact that D_p increased and then decreased as the echo area was increasing indicates that, for these days, D_p did not maintain a simple relation with echo area.

The results of this present study are compared to values of D_p from earlier studies in different climatic regions in Table 1. The comparison shows that this study produced results very similar to those reported by Lovejoy (1982) and Rys and Waldvogel (1986), indicating that, to a large extent, this scaling parameter is independent of geographical location. This conclusion is supported by an observation by Over and Gupta (1994), who reported that convective rain patterns in tropical ocean environments have similar scaling characteristics to patterns that occur over midlatitude land areas during the summer. The values of D_p are also very similar to those computed by Shook and Gray (1996, personal communication) for shallow snow covers during melt conditions on flat agricultural land.

Given the possible importance of echo size on the value of D_p, the time variation in this parameter is shown in Fig. 10 for only those echoes with areas of 200 km^2 or greater. This graph indicates that the value of D_p is larger (average value is 1.50 ± 0.32) when only the larger area echoes are considered (i.e., larger echoes tend to have greater edge variability than smaller echoes). The values of r^2 for the regression

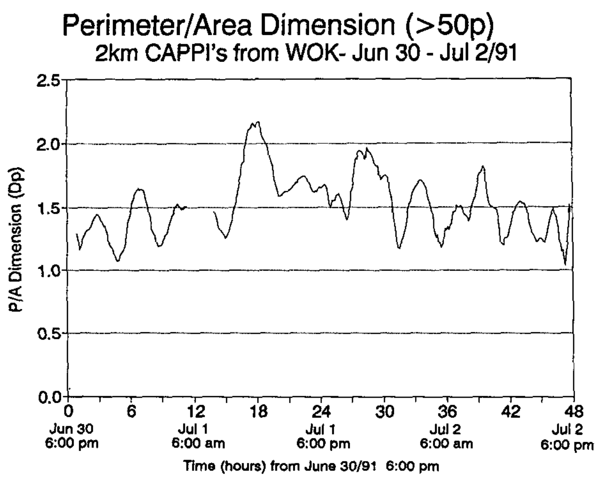

FIG. 10. Moving average variations in D_p for a rain intensity threshold of 0.2 mm h^{-1} for echoes greater than 200 km^2 during a 48-h period from 1800 LST 30 June to 1800 LST 2 July 1991. Moving averages were obtained from a 1-h centered running mean calculation.

lines for larger echoes on the CAPPI maps averaged 0.92, with lower values occurring on individual CAPPI maps when the number of echoes was low. This result suggests that the goodness of fit for the slopes of lines describing log area versus log perimeter were not as reliable for the large echoes as the values computed for the entire ensembles. Values of D_p greater than 2.0 were computed for the period from 1000 to 1200 LST 1 July when a few very large echoes were present. Such large values of D_p were unexpected. However, they occurred when "ragged" holes were present in the interior of the large echoes, giving the echoes a donut shape. As these interior holes grew, they increased the total length of the perimeter and decreased the area until the pattern became so fragmented that it consisted of a number of smaller echoes. These results provide confirmation that the presence of smaller echoes tended to decrease the value of D_p and higher values of D_p signal the presence of larger irregular echoes in the pattern, such as those found in the dissipation of a widespread, interconnected rain system. They also suggest that values of D_p likely decreased during the afternoons due to the formation of a number of small well-defined echoes associated with convective clouds.

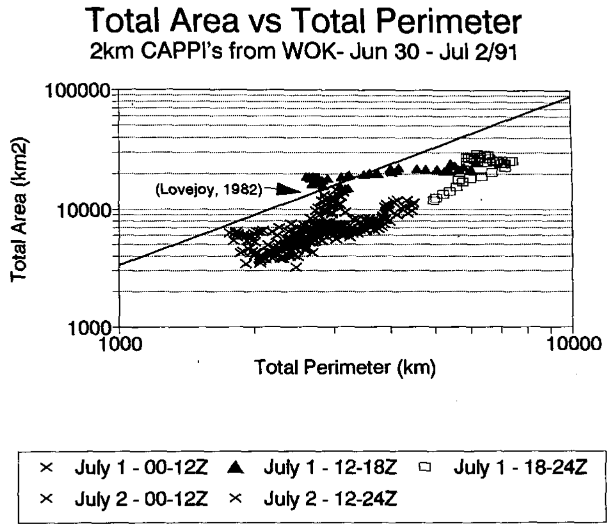

FIG. 11. Scattergraph showing the plots of perimeter and area for each ensemble and the perimeter/area relationship reported by Lovejoy (1982). The times when the total echo area increased and decreased rapidly on 1 July are marked with triangles and empty boxes.

In order to assess graphically the possible effects of synoptic condition on the perimeter/area ratio, the values of total echo perimeter and area for each CAPPI map were plotted (Fig. 11). To discriminate between periods of different echo behavior, triangles were plotted on the graph for the period when echo areas were increasing rapidly; empty boxes were used for the time period when echo areas were decreasing rapidly and crosses were used where the rates of change were less dramatic. To facilitate comparisons with earlier studies, the line of fit which Lovejoy (1982) obtained from his data is also shown on this scattergraph. According to Fig. 11, there were times when many of the CAPPIs with ensemble echo perimeters in the 1800–2600-km range had similar log perimeter to log area ratios. However, between 0300 LST (0900 UTC) and 0830 LST (1430 UTC) 1 July, ensemble echo perimeters varied relatively little ranging between 2600 and 3224 km, while total echo areas ranged from 8792 to 19 264 km^2. The largest echo areas associated with perimeters in this range occurred between 0600 LST (1200 UTC) and 0800 LST (1400 UTC) 1 July. Subsequently, large increases in ensemble echo perimeters occurred between 0830 LST (1430 UTC) and 1300 LST (1900 UTC), with a much smaller rate of percentage increase in echo area. The large increases in perimeter length occurred when interior holes formed in the larger echoes as they began to dissipate. In general, the points lay on a line that is similar to the slope of the line reported by Lovejoy (1982). However, the slope of a line through the points for ensembles between 0600 LST (1200 UTC) and 1200 LST (1800 UTC) 1 July (shown by triangles), when the effects of the low-level convergence on rain development was most dramatic, was very different from the slope of the line of best fit for all the data points. On the other hand, the slope of a line of best fit associated with the points while the storm system was dissipating would also have been different from the value reported by Lovejoy (1982). This observation demonstrates that atmospheric conditions can exert a significant influence on the scaling of the perimeter/area relationship.

One possible factor that could contribute to lower perimeter/area parameter values while the area remained relatively large (for example, for the period from 0600 to 1200 LST 1 July) are the smooth edges attributed to echoes that overlap the boundary of the study area. The effect of the smooth boundaries of the domain on total ensemble echo perimeters and the values of D_p was assessed by calculating an adjustment factor that accounted for the additional boundary perimeter associated with a "rough" echo and adding this value to the perimeters of echoes that overlapped the boundary of the study area. An adjustment factor was used rather than deriving the additional perimeter length from D_p to ensure that an independent check was carried out on the sensitivity of D_p to this edge effect.

In order to determine the adjustment factor, echoes overlapping the edges were analyzed at nine different times chosen to represent the range of echo patterns observed during the 2-day period. A number of straight line segments were fitted to form boundaries for these echoes. The perimeters for these straight line segments were compared to the perimeters for the echoes over the same distance. On average, the perimeters of the real echoes were 1.4 times as large as the length of the straight line segments. Based on this finding, the lengths of smooth edge perimeters were multiplied by

1.4 and these numbers were added to the total ensemble perimeters in place of the lengths of the straight edge segments of echoes overlapping the edge of the domain. Modified values of D_p were then computed for echo ensembles with a 0.2 mm h^{-1} threshold.

The results gave a new mean value for D_p of 1.353 (up slightly from 1.346) and a small increase in the standard deviation of D_p from 0.0425 to 0.0432. Since these changes lead to no significant changes in the results, it was concluded that the effects of smooth edges at the boundary of the study area did not need to be accounted for further.

b. *Korcak parameter*

The Korcak parameter represents the way in which the total area of echoes in the ensemble is distributed among the individual entities. Values of D_k ranged from 0.66 to 1.34 and averaged 1.07 ± 0.12. The correlation between points and the line of best fit between $F(A)$ and A was very good, with an average r^2 of 0.94, although not quite as good as the best fit for the regression lines involved in the calculations of D_p.

Figure 12 shows the 1-h centered running mean values for D_k. This parameter was influenced by the number of echoes, with higher values tending to occur when the total number of echoes was larger and lower values occurring when the total number of echoes was smaller. The values of D_k were lowest when most of the precipitation mass was concentrated in one or two large echoes, with a few additional small echoes present. The Korcak parameter appeared to be sensitive to afternoon convective activity because it generally increased during the afternoons.

As indicated in Figs. 9 and 12, the scaling properties for rain patterns are not static. This is not surprising since this study has shown they are sensitive to time variations in the underlying physical processes and, in turn, to the larger-scale synoptic processes.

Inspection of Fig. 12 shows that D_k is more variable than D_p. Furthermore, on several occasions when D_p reached a relative maximum, D_k was either decreasing or at a relative minimum. The correlation between D_p and D_k for the 377 ensembles with a 0.2 mm h^{-1} rain intensity threshold was −0.40 (significant at the 99% level). This would suggest that, for this particular period, rough echo edges (D_p large) were more likely to occur when there were one or two large echoes surrounded by a few smaller echoes (D_k small). It should be noted that the existence of a statistically significant negative correlation between D_p and D_k for 1 and 2 July should not be extrapolated to other days without additional analysis.

c. *Effect of intensity threshold*

The analysis of the echo ensembles was repeated using different rain intensity thresholds for defining echo and no-echo pixels. The thresholds included 0.5, 1.0, 2.0, 5.0, and 10.0 mm h^{-1} rain rates. As the intensity threshold increased, echo shapes changed and the weaker echoes disappeared. The effects of reflectivity threshold on rain area and on the average number of distinct cells are shown in Figs. 13a and 13b, respectively. The area of echo coverage decreased with increasing intensity level for intensities greater than 0.5 mm h^{-1}. The largest decreases occurred between the 1.0 and 5.0 mm h^{-1} intensity thresholds during the time interval from 0900 to 1600 LST 1 July when the area was under the influence of the trough and its associated zone of convergence.

The times when the maximum number of echoes occurred for different rain intensity thresholds were not always in phase. In particular, the peak in the number of echoes for the 1 mm h^{-1} threshold occurred at 1450 LST 1 July, while the peak for the 0.2 mm h^{-1} threshold did not occur until 1756 LST on the same day. At the 5 mm h^{-1} intensity threshold, the discrete rain cells embedded in larger echoes became more distinct, causing the total number of echoes for this threshold to increase to a maximum of 151 at 1243 LST 1 July when the rain area was also near its maximum.

The relationship between the average value of D_p and the intensity threshold is shown in Fig. 13c. As the intensity threshold increased, the average value of D_p remained relatively constant. However, the values of D_p for higher rain intensity thresholds were more variable with time. The relatively small changes in D_p with echo intensity indicates that the perimeter/area scaling property of rain events included in this study are similar over a range of intensities.

Figure 14 shows the time variation in D_p for echo ensembles with intensity thresholds of 0.2, 1.0, 5.0, and 10.0 mm h^{-1}. The curve for the 10 mm h^{-1} threshold

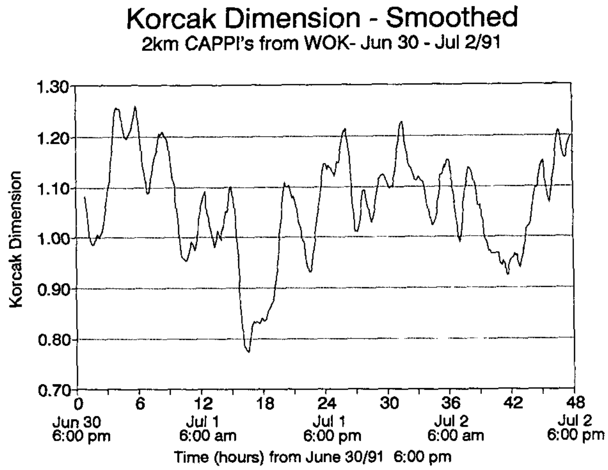

FIG. 12. Moving average variations in the Korcak parameter D_k over a 48-h period from 1800 LST 30 June to 1800 LST 2 July 1991. Moving averages were obtained from a 1-h centered running mean calculation.

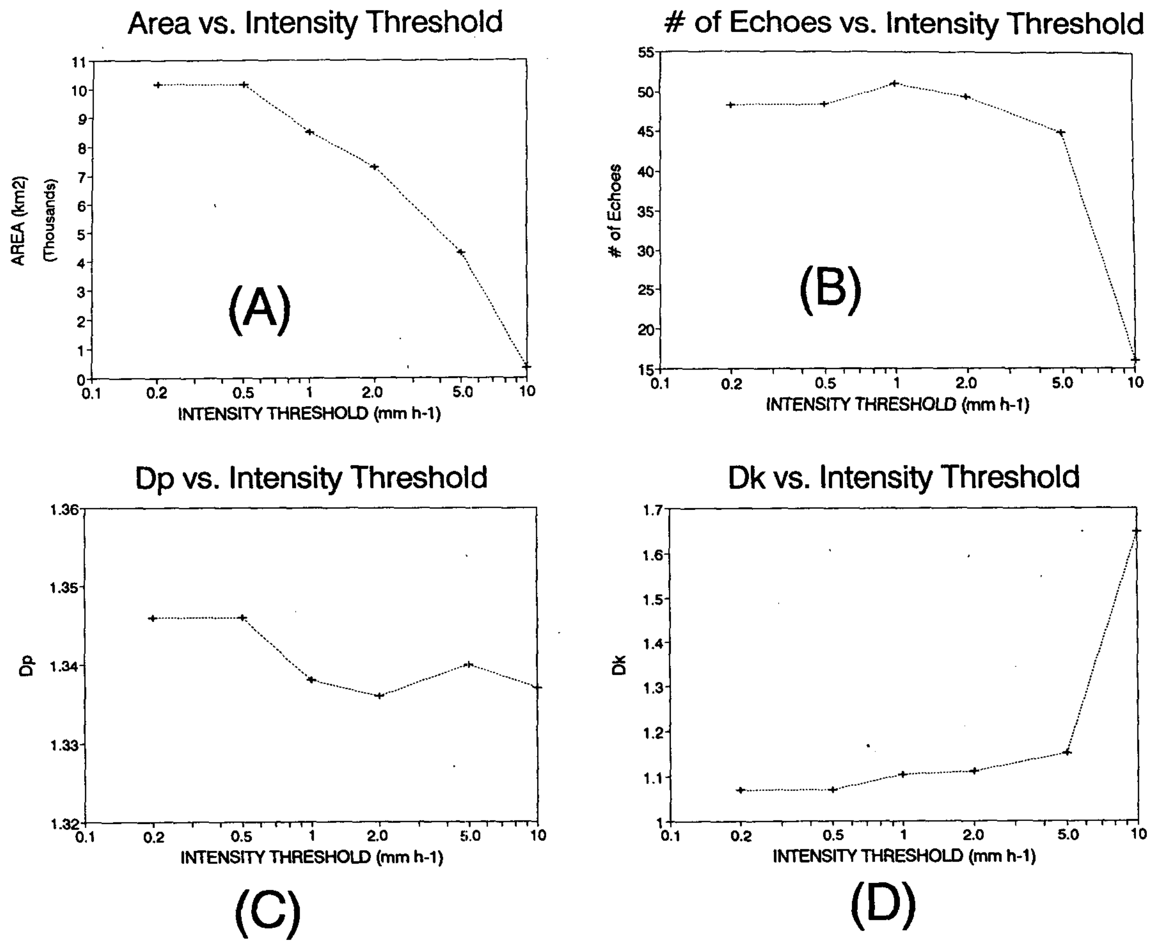

FIG. 13. The variations of (a) average echo area, (b) average number of distinct cells, (c) average perimeter/area parameter, and (d) average Korcak parameter, with different rain intensity thresholds.

is discontinuous because there were times when the number of high intensity cells was insufficient to reliably compute D_p. Values of D_p varied aperiodically with time for all intensity thresholds, and the pulsations were not in phase for the different intensity thresholds. Not surprisingly, the variability of D_p for the 10 mm h^{-1} intensity threshold was greater than its variability for lower thresholds. For lower intensity thresholds, values of D_p were higher in the morning of 1 July and decreased during the afternoon.

Figure 13d shows the variation in D_k with increasing intensity thresholds. It shows that the average value of D_k increased slightly with intensity threshold, although it remained relatively constant for thresholds less than 5.0 mm h^{-1}. Above this intensity threshold, the average value of D_k increased quite rapidly, in part because of the limited number of echoes at certain times.

The smoothed values of D_k showed similar values for each rain intensity threshold up to 5 mm h^{-1}, although at certain times the values of D_k for the 5 mm h^{-1} threshold were as much as 0.3 higher than the values for the 0.2 mm h^{-1} threshold. Figure 15 shows the moving average values of D_k for four different intensity thresholds. In general, the peaks on the graphs for 1 and 5 mm h^{-1} occurred simultaneously, although the amplitudes of the peaks was higher for the higher intensity thresholds. These results indicate that D_k is relatively stable with intensity threshold, although less so than D_p.

8. Conclusions

Rain patterns arising from large-scale moisture convergence associated with a deepening cold low on 1 July and forming on 2 July as a result of more localized convective processes were observed on a continuous basis by a C-band radar located at Elbow, Saskatchewan. During the period on 1 July when rain formation was enhanced by low-level moisture convergence, the echo area increased dramatically to as much as 50% coverage of the domain. Subsequently, as this convergence weakened, the echo area decreased and covered

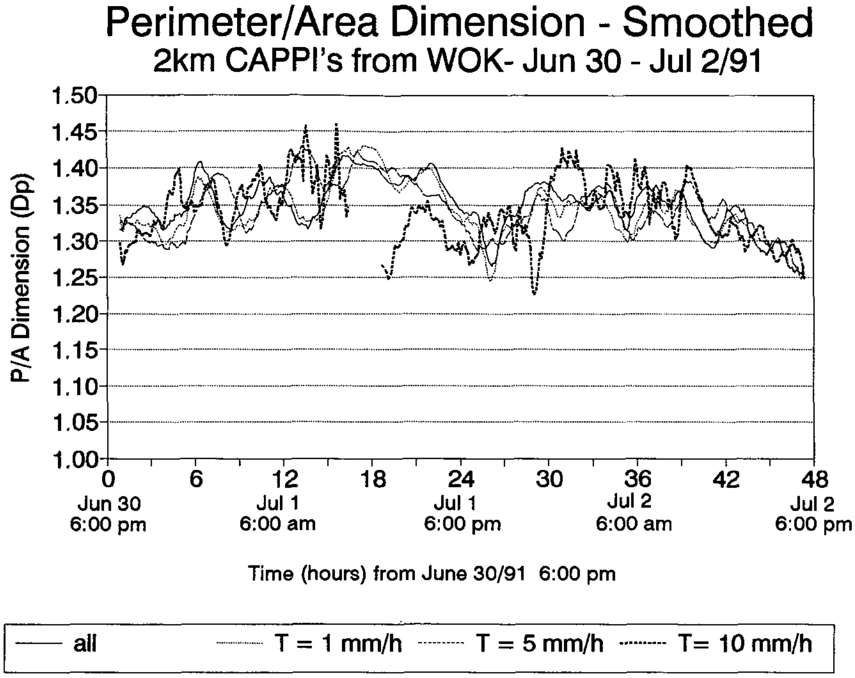

FIG. 14. Moving average variations in the values of D_p with different rain intensity thresholds during a 48-h period from 1800 LST 30 June to 1800 LST 2 July 1991. Moving averages were obtained from a 1-h centered running mean calculation.

7%–14% of the study area for the remainder of 1 and 2 July. In spite of the much more extensive echo coverage on 1 July, the maximum rain flux on 2 July was within 20% of the maximum rain flux on 1 July.

The scaling properties of these rain patterns were explored in this study by an analysis of the perimeter/area scaling parameter. The value of the perimeter/area parameter (D_p) for rain patterns on 2-km MSL CAPPI maps ranged from 1.22 to 1.46 and averaged 1.35 $\pm$ 0.04 through the 48-h study period for the lowest intensity threshold (0.2 mm h^{-1}). The values of D_p were very reliable throughout the 48-h study period, as indicated by the values of r^2 that showed little variation from their average value of 0.98. The average value of D_p for this study agrees with the values reported in other studies of clouds and rain patterns. Furthermore, the average value of D_p remained relatively constant with increasing rain intensities for thresholds up to 5.0 mm h^{-1}, indicating that the choice of intensity threshold is not a critical factor in the analysis of the scaling properties of rain echoes. Ensembles composed only of rain echoes with areas greater than 200 km^2 have higher values of D_p, indicating that this parameter is likely to be larger for larger echoes. For this study, the trend was particularly evident when the echoes were dissipating.

The results of this study indicated that the relationship between ensemble echo area and echo perimeter is dependent on the synoptic condition, which implies that the scaling properties of rain echoes were affected by the atmospheric processes controlling rain formation. The scaling properties of rain echo ensembles were dependent to a certain extent on the rates of growth and dissipation of echoes. Furthermore, in the case of widespread rain, changes in D_p appeared to precede visible changes in the overall pattern. In addition, time variations in D_p were associated with variations in the more conventional echo ensemble statistics such as echo area and number of echoes.

The Korcak (D_k) parameter is more variable in time than D_p. For this 48-h period D_k ranged from 0.66 to 1.34 with an average value of 1.07 $\pm$ 0.13 for an intensity threshold of 0.2 mm h^{-1}. Average values of D_k are generally stable for rain intensity thresholds up to and including 5 mm h^{-1}. However, during periods of widespread rain, D_k tended to be lower for lower intensity thresholds. In addition, a statistically significant negative correlation existed between D_p and D_k for this study period.

In summary, the time variations of the simple scaling parameters considered in this study are dependent on the physical processes giving rise to the rain patterns, which indicates that, when combined with other ensemble properties such as echo area, they have the potential to be useful indicators of mesoscale atmospheric processes.

9. Future research and application

When combined with information on the synoptic conditions, scaling parameters can provide a means of

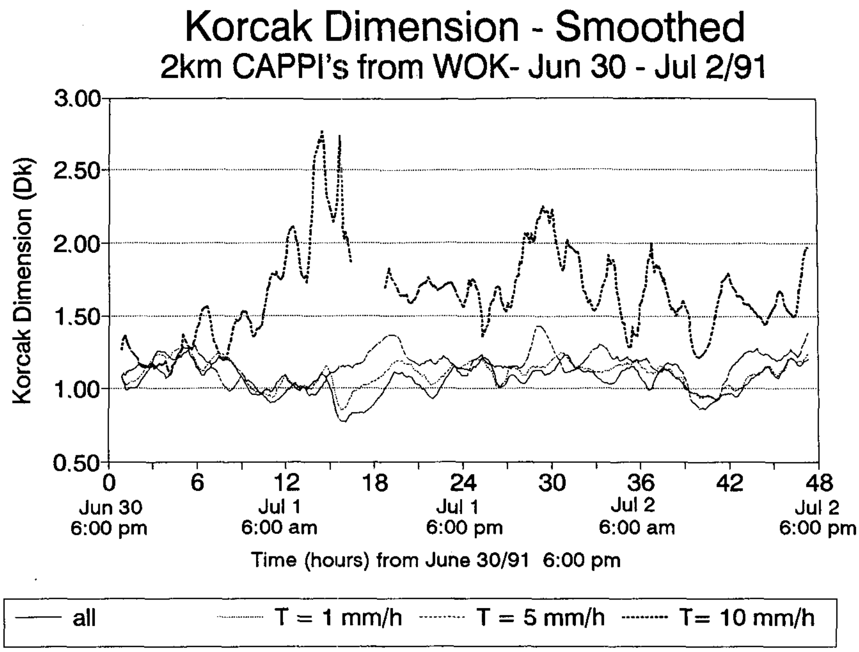

FIG. 15. Moving average variations of D_k associated with different rain intensity thresholds during a 48-h period from 1800 LST 30 June to 1800 LST 2 July 1991. Moving averages were obtained from a 1-h centered running mean calculation.

monitoring and, possibly, predicting the spatial characteristics of rain patterns. For example, changes in D_k that occur with the onset of convection may be a useful way of characterizing the presence and extent of convection over the area of radar coverage. If a relationship can be developed between changes in specific echoes and the scaling properties of large-scale rain patterns, then it may be possible to forecast the probable changes in rain patterns and echo ensembles given the large-scale instability, moisture convergence, and shear conditions. Consequently, future research will be directed at establishing relationships between the scaling properties of echo shapes and both the internal geometric properties of the echoes and the external environmental parameters. In addition, studies of the ensemble growth and dissipation in terms of multifractal dimensions may provide a more rigorous definition of these scaling properties, as well as effective procedures for incorporating these properties of rain patterns into hydrological models.

Acknowledgments. The author would like to acknowledge the important contribution of Dr. Kevin Shook, who made his analysis software available for carrying out this study and provided advice on its implementation. The contributions of Mr. Dan Magosse in modifying the program and, especially, those of Mr. Ray Keller in preparing the radar datasets for analysis and in processing the data are also gratefully acknowledged. In addition, comments by Mr. Joe Eley and Drs. Kevin Shook and Don Gray and the reviewers have been helpful in fine-tuning this paper.

REFERENCES

Browning, K. A., M. E. Hardman, T. W. Harrold, and C. W. Pardoe, 1973: The structure of rainbands within a midlatitude depression. *Quart. J. Roy. Meteor. Soc.,* **99,** 215–231.

Chisholm, A. J., and J. H. Renick, 1972: The kinematics of multicell and supercell Alberta hailstorms. *Alberta Hail Studies,* Alberta Research Council Hail Studies Rep. 72-2, 24–31.

Entekhabi, D., and P. S. Eagleson, 1989: Land surface hydrology parameterization for atmospheric general circulation models including subgrid scale spatial variability. *J. Climate,* **2,** 816–831.

Gupta, V. K., and E. C. Waymire, 1993: A statistical analysis of mesoscale rainfall as a random cascade. *J. Appl. Meteor.,* **32,** 251–267.

Halsey, T. C., M. H. Jensen, L. P. Kadanoff, I. Procaccia, and B. I. Shraiman, 1986: Fractal measures and their singularities. The characterization of strange sets. *Phys. Rev. A,* **33,** 1141–1151.

Hentschel, H. G. E., and I. Procaccia, 1984: Relative diffusion in turbulent media: The fractal dimension of clouds. *Phys. Rev. A,* **29,** 1461–1470.

Johnson, L. R., and P. L. Smith, 1990: Estimation of convective rain volumes utilizing the area-time-integral technique. Preprints, *Eighth Conf. on Hydrometeorology,* Kananaskis Park, AB, Canada, Amer. Meteor. Soc., 165–168.

Kumar, P., and E. Foufoula-Georgiou, 1994: Characterizing multiscale variability of zero intermittency in spatial rainfall. *J. Appl. Meteor.,* **33,** 1516–1525.

Lovejoy, S., 1982: The area–perimeter relation for rain and cloud areas. *Science,* **216,** 185–187.

——, and D. Schertzer, 1990: Multifractals, universality classes and satellite and radar measurements of cloud and rain fields. *J. Geophys. Res.*, **95**(D3), 2021–2034.

——, and ——, 1991: Multifractal analysis techniques and the rain and cloud fields from 10^{-3} to 10^{6} m. *Nonlinear Variability in Geophysics-scaling and Fractals,* D. Schertzer and S. Lovejoy, Eds., Kluwer Academic Publishers, 111–144.

Mandelbrot, B. B., 1983: *The Fractal Geometry of Nature.* W. H. Freeman and Co., 468 pp.

Marshall, J. S., and W. McK. Palmer, 1948: The distribution of rain drops with size. *J. Meteor.,* **V,** 165–166.

Over, T. M., and V. K. Gupta, 1994: Statistical analysis of mesoscale rainfall: Dependence of a random cascade generator on large-scale forcing. *J. Appl. Meteor.,* **33,** 1526–1542.

Reyni, A., 1970: *Probability Theory* (English translation by I. Vekerdi). North-Holland series in applied mathematics and mechanics, Vol. 10, 666 pp.

Rys, F. S., and A. Waldvogel, 1986: Fractal shape of hail clouds. *Phys. Rev. Lett.,* **56,** 784–787.

Schertzer, D., and S. Lovejoy, 1987: Physical modeling and analysis of rain and clouds by anisotropic scaling of multiplicative processes. *J. Geophys. Res. D,* **92**(8), 9693–9714.

Shook, K., 1993: Fractal geometry of snowpack during ablation. M.S. Thesis, Dept. of Engineering, University of Saskatchewan, 178 pp.

Wang, Q., and R. G. Lawford, 1994: Multifractals in precipitation in Saskatchewan. *Program and Abstracts, Int. GCIP/MAGS Workshop on Scaling in Hydrometeorological/Hydrological Processes and Models,* Victoria, BC, Canada, National Hydrology Research Centre, 34.

Zawadzki, I., J. Morneau, and R. Leprise, 1994: Predictability of precipitation patterns: An operational approach. *J. Appl. Meteor.,* **33,** 1562–1571.